International Journal of Minerals, Metallurgy and Materials
Volume 29, Number 2, February 2022, Page 271
https://doi.org/10.1007/s12613-020-2156-3

Effect of 2-mercaptobenzothiazole concentration on sour-corrosion behavior of API X60 pipeline steel: Electrochemical parameters and adsorption mechanism

Masoud Sabzi[1),✉], *Amir Hayati Jozani*[2)], *Farzad Zeidvandi*[2)], *Majid Sadeghi*[3)], *and Saeid Mersagh Dezfuli*[2)]

1) Young Researchers and Elite Club, Dezful Branch, Islamic Azad University, Dezful, Iran
2) Department of Materials Science and Engineering, Science and Research Branch, Islamic Azad University, Tehran, Iran
3) Center of Excellence for Surface Engineering and Corrosion Protection of Industrial, School of Metallurgy and Materials Engineering, College of Engineering, University of Tehran, P.O. Box 11155-4563, Tehran, Iran
(Received: 17 May 2020; revised: 12 July 2020; accepted: 28 July 2020)

Abstract: We investigated the effect of the 2-mercaptobenzothiazole concentration on the sour-corrosion behavior of API X60 pipeline steel in an environment containing H_2S at 25°C and in the presence of 0, 2.5, 5.0, 7.5, and 10.0 g/L of 2-mercaptobenzothiazole inhibitor. To examine this behavior, we conducted open-circuit potential (OCP), potentiodynamic polarization, and electrochemical impedance spectroscopy (EIS) tests. Energy dispersive spectroscopy and scanning electron microscopy were also used to analyze the corrosion products. The results of the OCP and potentiodynamic polarization tests revealed that 2-mercaptobenzothiazole reduces the speed of both the anodic and cathodic reactions. An assessment of the Gibbs free energy of the inhibitor ($\Delta G^{\ominus}_{ads}$) indicated that its value was less than −20 kJ·mol^{-1} and greater than −40 kJ·mol^{-1}. Therefore, the adsorption of 2-mercaptobenzothiazole onto the surface of the API X60 pipeline steel occurs both physically and chemically, the latter of which is particularly intentional. In addition, as the $\Delta G^{\ominus}_{ads}$ value was negative, we could conclude that the adsorption of 2-mercaptobenzothiazole onto the surface of the pipeline steel occurs spontaneously. The EIS results indicate that with the increase in the 2-mercaptobenzothiazole inhibitor concentration, the corrosion resistance of API X60 steel increases. An analysis of the corrosion products revealed that iron sulfide compounds form on the surface. In summary, the results showed that an increase in the inhibitor concentration results in a decrease in the corrosion rate and an increase in inhibitory efficiency. Additionally, we found that the 2-mercaptobenzothiazole adsorption process on the API X60 steel surfaces in an H_2S-containing environment follows the Langmuir adsorption isotherm and occurs spontaneously.

Keywords: API X60 steel; sour corrosion; 2-mercaptobenzothiazole; inhibitor concentration; electrochemical parameters; environments containing hydrogen sulfide

1. Introduction

Corrosion in industries such as the oil and petrochemical industries imposes enormous annual costs for the replacement or repair of machinery. Annually, the gross national product (GDP) values of countries around the world are reduced by nearly five percent due to corrosion. About a fifth of this wasted GDP is in the oil and gas and petrochemical industries. One type of corrosion in oil and gas industries is that caused by hydrogen sulfide (H_2S) gas. Many oil and gas installations are constructed of carbon and stainless steel, which are subject to corrosion by H_2S gas. In fact, H_2S causes a variety of types of corrosion in these steels [1–3]. This colorless odorous gas, which is soluble in water, oil, and alcohol, has a fairly sweet taste. H_2S is a weak acid, is very toxic to humans, and can cause metallic corrosion when dissolved in water [4–5]. Oil wells with an H_2S content higher than 10 ppm in the soluble phase are referred to as sour wells [5–7].

If an acid gas contains H_2S, the primary corrosion product will be iron sulfide, which produces a film with poor adhesion. However, although the ability to protect an iron sulfide layer is better than that of iron carbonate, but for the iron sulfide film to be shielded, the H_2S content must be sufficient [7–8]. The overall reaction of sour corrosion is as follows [9]:

$$Fe_{(s)} + H_2S_{(g)} = FeS_{(s)} + H_{2\,(g)} \quad (1)$$

The corrosion of pipeline steels in the presence of H_2S poses many problems for oil, gas, and petrochemical plants. In these conditions, the formation of surface layers (corrosion products) on metal surfaces is very effective in mitigating the corrosion rate. The growth of these layers is strongly dependent on the kinetics of their formation [9–11]. Different types of iron sulfide may form in the presence of H_2S, including cubic ferrous sulfide (FeS), mackinawite, amorphous FeS, and troilite [11–13]. In certain environmental conditions, these layers will form on the surface and their relative stability can be determined. Previous studies have shown that these corrosion products can convert to one or another if the necessary thermodynamic conditions are present. These sulfide shells exhibit different shielding properties, with the

✉ Corresponding author: Masoud Sabzi E-mail: mas.metallurg88@gmail.com

highest protection potential being that of pyrite, followed by pyrrhotite, troilite, and mackinawite. The protective nature of these shells, in terms of the morphology (amorphous or polycrystalline) and composition of th e corrosion products, depends on factors such as the H_2S concentration in the solution, pH, and temperature [14–15]. If sulfur is present in the system at a high concentration, a pyrite phase forms. Pyrrhotite is a non-stoichiometric form of FeS found in the sourest environments. The third available form of FeS is mackinawite, which is a semi-stable form of FeS that occurs in all conditions, especially in environments with low H_2S activity. In addition, sulfide films in environments with a pH above 6 and high concentrations of H_2S have been found to have very poor shielding properties despite the presence of a dominant mackinawite phase. It is commonly observed that as the concentration of this component increases, the protective properties of the surface films are lost [16–18].

Due to the diversity of corrosion mechanisms, the methods used for corrosion protection also differ [19–26]. Obviously, effective corrosion protection methods must be designed based on the nature of the active corrosion factors [25–30]. The most important corrosion control methods in the field of sour-gas transportation involve the use of micro-alloy steel tubes with special grades of gas pipeline transportation, internal corrosion protection coatings, injection of corrosion inhibitors, and cathodic protection. We note that the above methods do not have the same levels of effectiveness. For example, corrosion inhibitors and cathodic protection are only applicable as auxiliary and support processes and cannot independently control corrosion in a gas-containing environment. On the other hand, pipelines made of micro-alloy steels or the application of polymer coatings in oil and gas pipelines can be designed and implemented as stand-alone solutions [31–32]. However, it has been empirically demonstrated that one of the relatively inexpensive methods for controlling sour corrosion is the use of corrosion inhibitors. For this reason, in recent years, extensive research has been conducted to determine the effectiveness of inhibitors on the corrosion behavior of different steels [33–34].

One of the important ways to protect pipeline steels is to use organic inhibitors. Many organic compounds that contain oxygen, sulfur, nitrogen, and multiple bonds are good inhibitors of different alloys. Azoles, which contain many constituents, are an example of this type. Important derivatives of azoles are mercapto-azole compounds, which have been recognized in recent years as highly effective inhibitors of various alloys. Inhibitors containing a mercapto group (–SH) can form stable complexes with iron ions via thiol bonding. The inhibition mechanism is based on the formation of complexes between the inhibitor and iron ions on the surface of the steel pipeline. The most important mercapto-azole compounds are mercaptobenzoxazole, mercaptobenzimidazole, and mercaptobenzothiazole [35–37]. In the past few years, the impact of inhibitors on the corrosion behavior of pipeline steels has been extensively investigated. Okonkwo *et al.* [38] investigated the effect of ambient temperature on the sour-corrosion behavior of API X80 steel pipeline and reported that as the temperature increases from 20 to 60°C, the sour-corrosion resistance of this alloy sharply decreases. Cen *et al.* [39] investigated the effect of 2-mercaptobenzothiazole on the corrosion behavior of a carbon steel and found 2-mercaptobenzothiazole to have a greater effect on supercritical CO_2 than on non-supercritical CO_2. Kartsonakiset *et al.* [40] investigated the effect on corrosion of applying 2-mercaptobenzothiazole coatings on steel. Their findings showed that the presence of 2-mercaptobenzothiazole in hybrid organic–inorganic coatings improved corrosion resistance.

Based on the above information, in this study, we used the 2-mercaptobenzothiazole inhibitor in various environments. We investigated the effect of the concentration of 2-mercaptobenzothiazole on the corrosion behavior of API X60 pipeline steel and characterized the electrochemical and thermodynamic parameters in an H_2S-containing medium. Previous researchers have not addressed this issue.

2. Experimental

The steel samples used in this study were API X60 pipelines consisting of wrought steel. For sampling purposes, we used a pipeline currently in operation in the oil industry. Using a spark emission spectrometer made in Germany, we determined the chemical composition of the steel, which is reported in Table 1. This type of steel is used in pipe construction to transport oil, gas, and water in the oil, gas, and petrochemical industries. To prepare steel specimens, we first produced steel pieces with the dimensions 1 cm × 1 cm × 1 cm. The steel pieces were then soldered to a copper wire. Next, the back and side surfaces and the joints of the specimens and copper wire were completely covered with epoxy resin so that the area of pipeline exposed to the electrolyte was 1 cm^2. Then, the bare surface of the steel samples was polished with sand paper of up to 1500 grit. The samples were then washed with acetone and dried at room temperature, followed by washing with double-distilled water and drying in air. They were then quickly subjected to open-circuit potential (OCP), potentiodynamic polarization, and electrochemical impedance spectroscopy (EIS) tests. The steel samples were then used as working electrodes in our electrochemical studies.

Table 1. Chemical composition of the steel samples in this investigation wt%

C	Mn	Si	P	S	V	Ti	Nb	Fe
0.16	1.39	0.43	0.02	0.01	0.07	0.04	0.05	Balance

As the corrosion inhibitor, we used 2-mercaptobenzothiazole manufactured by Merck, Germany. Fig. 1 shows the chemical structure of this inhibitor.

To prepare the solution containing H_2S gas, we first prepared Na_2S, Na_2SO_4, H_2SO_4, and distilled water. To investigate sour corrosion, we injected neutral gas into the solution to remove oxygen, and prior to each test, the 1 M Na_2SO_4 solu-

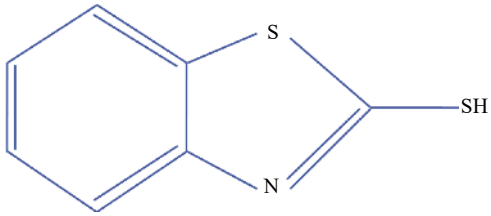

Fig. 1. Chemical structure of 2-mercaptobenzothiazole compound.

tion was purified with argon for 30–45 min. In this way, several cathodic reactions (oxygen reduction) could be performed in the solution. Then, using H_2SO_4, the pH of the 1 M Na_2SO_4 solution was increased up to three times. Lastly, the required amount of Na_2S was added to reach an H_2S concentration of 10–20 ppm. As shown in Eq. (2), Na_2S will dissolve and produce H_2S gas [41]:

$$Na_2S + 2H^+ \rightarrow 2Na^+ + H_2S \quad (2)$$

As small amounts of H_2S gas, i.e., approximately 10–20 ppm, form near the surface of the working electrode, the argon gas and dissolved oxygen must be depleted during the electrochemical experiments. Then, we added 0, 2.5, 5.0, 7.5, or 10.0 g/L 2-mercaptobenzothiazole inhibitor to the prepared solutions. Finally, to investigate the sour-corrosion behavior of the API X60 pipeline steel under these conditions, we performed OCP, potentiodynamic polarization, and EIS measurements after 2 h of immersion in the designed environment. We also note that we measured the final pH of the corrosive medium with an electronic pH meter, the value of which was (5.1 ± 0.2). The time required for the corrosion cell to reach stability was 120 min, which ensured that the OCP fluctuation was at a minimum. Corrosion tests were conducted at a temperature of 25°C using an AMETEK potentiostat (Model 2273 PARSTAT) with a standard three-electrode tube containing the Ag/AgCl electrode as the reference electrode, a platinum rod as the auxiliary electrode, and the test samples as the working electrodes. We note that the potentiodynamic polarization test was performed in the range of (−1000 ± 100) to (1000 ± 100) mV relative to the OCP with a scanning rate of 1 mV/s. After performing the first OCP measurement, we performed the EIS measurements at the OCP, an amplitude of 10 mV, and a frequency range of 10 mHz–100 kHz. Each test was repeated three times in the designed environment to ensure the repeatability of the results in the sour-corrosion environment, after which, the corrosion test results were analyzed using Zview2 software. In each experiment, we used a fresh solution and controlled the temperature using a thermostat. For each electrochemical test, we calculated the inhibition efficiency (IE), surface coverage (θ), and corrosion rate in mm/a. In addition, we used energy dispersive spectroscopy (EDS) and scanning electron microscopy (SEM) to analyze the morphology and surface corrosion products of the samples. Given that the potentiodynamic polarization test is destructive, the sequence of these electrochemical tests was as follows: first, we performed the OCP test, followed by the EIS test, and then the potentiodynamic polarization tests.

3. Results and discussion

3.1. Open-circuit potential

The OCP or equilibrium potential is the potential of the sample in the absence of a current. Before conducting corrosion tests, sufficient time must be allowed for the electrochemical cells to achieve stable conditions with little change in potential. In some cells, these stable conditions occur after a few minutes and in others after a few hours [42–45]. The corrosion current in an open circuit can be also measured. In electrochemical tests, the potential of open-circuit steel in the electrolyte is typically performed first to ensure the environmental stability of the steel. Then, other electrochemical tests are based on information obtained from the OCP of the steel in that particular environment. When pipeline steel or any other material is placed in an electrolyte, the OCP value changes over time. This is because it takes a certain amount of time for an oxide layer to form on the surface of that alloy or fragment as an electrical double layer. Ostensibly, how the OCP of a steel pipeline changes over time depends on several factors. The time required to reach the OCP of an alloy at a constant value depends on the type of alloy and the chemical composition of the electrolyte [46].

The OCP tests were conducted without an inhibitor and then with the addition of 2.5, 5.0, 7.5, or 10.0 g/L of the 2-mercaptobenzothiazole inhibitor at 25°C. Fig. 2 shows the results of these tests, in which we can see that by reducing the concentration of the 2-mercaptobenzothiazole inhibitor, the OCP shifted to more negative values. This reflects the greater activity of API X60 steel dipped in the H_2S-containing environment due to the increased level of corrosive ion attacks. In fact, this indicates that reducing the 2-mercaptobenzothiazole inhibitor concentration increases the susceptibility of API X60 pipeline steel to corrosion in an H_2S-containing environment. This finding is highlighted by the shift of the API X60 pipeline surface potential to more negative values. The main factor explaining this result is that the concentration of the 2-mercaptobenzothiazole inhibitor changes the structure of the electrical double layer. It also changes the concentration of the reduction–oxidation species near the

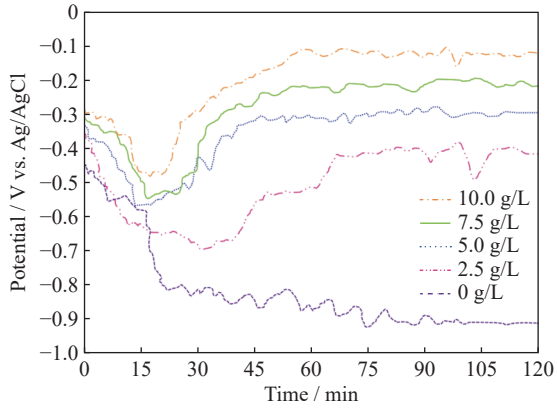

Fig. 2. Effect of 2-mercaptobenzothiazole concentration on the OCP diagrams of API X60 steel in an H_2S-containing environment.

surface of the API X60 pipeline steel.

Examination of Pourbaix diagrams for an H_2S–H_2O double system shows that H_2S gas has a relatively wide range of stability. In solutions containing H_2S gas, the cathodic reaction occurs as follows [47]:

$$2H_2S + 2e^- \rightarrow H_2 + 2HS^- \quad (3)$$

This reaction is limited by the penetration of H_2S into the solution and by the excess voltage of H_2. The reaction shown in Eq. (3) has two steps that occur as follows:

$$H_2S + e^- \rightarrow H^0 + HS^- \quad (4)$$

$$H_2S + H^0 + e^- \rightarrow H_2 + HS^- \quad (5)$$

This mechanism indicates that upon initial adsorption of H_2S, the metal surface is directly decomposed into atomic hydrogen and disulfide ions. At higher cathode voltages, most of the HS^- ions are decomposed. The decomposition reaction of these ions is as follows:

$$2HS^- + 2e^- \rightarrow H_2 + 2S^{2-} \quad (6)$$

This reaction also occurs in two steps:

$$HS^- + e^- \rightarrow H^0 + S^{2-} \quad (7)$$

$$HS^- + H^0 + e^- \rightarrow H_2 + S^{2-} \quad (8)$$

The anodic reaction for the API X60 pipeline steel in the sour solution is a dissolution reaction of metallic iron and its conversion to iron ions, which occurs in the following steps:

$$Fe + HS^- \rightarrow FeHS^- \quad (9)$$

$$FeHS^-_{ads} \rightarrow FeHS^+ + 2e^- \quad (10)$$

$$FeHS^+ \rightarrow Fe^{2+} + HS^- \quad (11)$$

According to Eqs. (3)–(11), the noticeable change in the OCP of the API X60 pipeline steel might be due to the higher activity of the HS^- and S^{2-} ions on the surface. The potentials of these ions in the solution were shown to shift to more active potentials. The reason for this is that in H_2S-containing solutions, changes in the concentrations of the oxidizing and reducing species are strongly dependent on the concentration of the inhibitor. Any change in the concentration of the inhibitor can have the effect of significantly increasing the concentration of the HS^- and S^{2-} ions on surface of the API X60 pipeline steel, hence intensifying the surface activity and iron dissolution [48–49].

To obtain the OCPs, the samples were immersed in H_2S solution for 120 min. As can be seen in Fig. 2, up to 15 min, the OCP values with a large slope shift to negative values. However, during the second time interval (15–40 min), the slope of the OCP changes with time. In the third stage (40–65 min), the OCP variations show an upward trend. These developments occurred in the third stage reflect the formation of a protective film on the surface of the API X60 pipeline steel. Finally, in the fourth zone, the slight changes in the slope reflect the stable conditions in the API X60 steel/solution and the creation of conditions suitable for conducting electrochemical tests. Moreover, we note that the formation of the protective film occurred only in the presence of a corrosion inhibitor. In the absence of corrosion inhibitor, the OCP during the test had a negative slope, indicating that no protective film had formed on the surface. Also, the OCP curves indicate that increasing the concentrations of 2-mercaptobenzothiazole in the H_2S solution reduced the anode penetration of API X60 steel, which means that 2-mercaptobenzothiazole delayed the cathodic reaction. It seems that by increasing the concentration of the 2-mercaptobenzothiazole inhibitor, more layers of coating occurred on the API X60 pipeline in the H_2S solution.

3.2. Potential dynamic polarization

Fig. 3 shows potentiodynamic polarization diagram for the API X60 pipeline steel in the H_2S-containing environment with and without the presence of different concentrations of 2-mercaptobenzothiazole. Table 2 also shows the electrochemical parameters obtained from the figure. We calculated the efficacy of the 2-mercaptobenzothiazole inhibitor (IE) based on the following relationship [50]:

$$IE = (1 - \frac{I_{corr}}{I^0_{corr}}) \times 100 \quad (12)$$

where I^0_{corr} and I_{corr} are the corrosion current densities obtained at the intersection of the anodic and cathodic regions

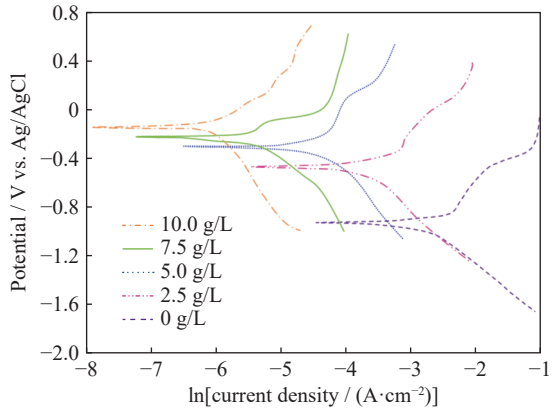

Fig. 3. Diagram of the influence of 2-mercaptobenzothiazole concentration on the polarization of API X60 pipeline steel.

Table 2. Influence of 2-mercaptobenzothiazole concentration on the electrochemical parameters of API X60 Steel

Inhibitor concentration / (g·L^{-1})	E_{corr} / mV vs. Ag/AgCl	I_{corr} / (μA·cm^{-2})	Corrosion rate / (mm·a^{-1})	IE	θ
0	−919 ± 8	63922 ± 7	1.325 ± 0.036	—	—
2.5	−804 ± 9	22823 ± 9	1.012 ± 0.071	64 ± 1	0.64
5.0	−306 ± 8	8228 ± 9	0.851 ± 0.039	87 ± 1	0.87
7.5	−227 ± 9	3887 ± 5	0.604 ± 0.034	94 ± 1	0.94
10.0	−151 ± 9	1661 ± 8	0.507 ± 0.027	97 ± 1	0.97

of the Tafel curves and the corrosion potential of the API X60 steel in an H_2S-containing environment, without and with different concentrations of 2-mercaptobenzothiazole, respectively. In addition, by dividing the IE value by 100, we obtained the degree of surface coverage (θ) by the inhibitor. As can be seen in Fig. 3, in the presence of 2-mercaptobenzothiazole, the corrosion current density decreased relative to that in the solution without the inhibitor. This indicates that the traditional 2-mercaptobenzothiazole reduced the anodic and cathodic reactions of the corrosion process. Also, the corrosion potential slowly shifted to negative values and the cathodic parts of the polarization graphs were clearly suppressed. This could be due to the fact that the 2-mercaptobenzothiazole inhibitor prevents the production of hydrogen. In Fig. 3, we can also see that in the presence of 2-mercaptobenzothiazole, the both cathodic and anodic currents decreased. In both Fig. 3 and Table 2, we can see that with increase in the concentration of the inhibitor, the corrosion rate and corrosion current density substantially decreased. Therefore, it can be said that 2-mercaptobenzothiazole can protect the surface of the pipeline steel against attack by corrosive ions in sour environments.

According to previous reports [51–53], if the corrosion potential in the presence of an inhibitor, as opposed to the absence of an inhibitor, is displaced more than 85 mV toward a more positive or negative potential, the inhibitor will be anodic or cathodic in type, respectively. However, if this displacement is less than 85 mV, the inhibitor will be considered to be mixed. A mixed inhibitor is one that simultaneously delays anodic or cathodic reactions, affecting the rate of both anodic (metal dissolution) and cathodic (conversion of H^+ to H_2) reactions involved in the corrosion process [54–56]. In this study, with increase in the concentration of 2-mercaptobenzothiazole in an H_2S-containing environment, the corrosion potential displacement was greater than 85 mV. Therefore, 2-mercaptobenzothiazole is considered to be an anode or cathode potential inhibitor in H_2S-containing environments for API X60 pipeline steel. As we can see in the potentiodynamic polarization diagrams in Fig. 3, increasing the concentration of the 2-mercaptobenzothiazole inhibitor in the solution shifted the corrosion potential (E_{corr}) to more positive values. This displacement exceeded 85 mV, which classifies 2-mercaptobenzothiazole as a cathodic or anodic corrosion inhibitor. Therefore, the results show that 2-mercaptobenzothiazole acts as a physical and chemical adsorption. These results also suggest that increasing the concentration of 2-mercaptobenzothiazole reduces anodic dissolution and delays hydrogen production.

3.3. Adsorption consideration

It is known that if the adsorption of molecules at a metal–soluble interface is the main reason for the adsorption of the corrosion inhibitor, then the adsorption isotherm should be investigated to understand the relationship between the inhibitor and the metal surface [57–60]. The surface adsorption of inhibitor molecules on a metal surface is a substitution process whereby the water molecules adsorbed onto the metal surface are replaced by inhibitor molecules [60–61]. Hence, to better understand the inhibitory adsorption mechanism and the electrochemical processes occurring on the surface of API X60 pipeline, we investigated the adsorption isotherms. We also determined the distributions of the inhibitor concentration in the electrolyte and on the surface of the API X60 pipelines by the adsorption isotherms. Of the several models available for obtaining adsorption isotherms, the most widely used is the Langmuir isotherm model.

Adsorption isotherms can be used to calculate the thermodynamic parameters involved in the adsorption of the inhibitors. In fact, Langmuir isotherms are based on the equilibrium of the total adsorption positions and the non-independent adsorption of the particles. With this assumption, the proportions of the surface coverage (θ) and the inhibitor concentration (C) are determined as shown in Eq. (13). In this equation, θ is unitless and K_{ads} is the adsorption–desorption equilibrium whose unit is the inverse of the concentration ($dm^3 \cdot mol^{-1}$), which is obtained using Eq. (14) [62–65].

$$K_{ads}C = \left(\frac{\theta}{1-\theta}\right) \tag{13}$$

$$\left(\frac{1}{K_{ads}}\right) + C = \frac{C}{\theta} \tag{14}$$

The degree of surface coverage, which is the ratio of the surface area coated by the inhibitor to the total metal surface available to adsorb the inhibitor, is obtained using Eq. (15) [62–65]:

$$\theta = \frac{IE}{100} = 1 - \frac{I_{corr}}{I^0_{corr}} \tag{15}$$

By plotting C/θ versus C (Fig. 4), a linear relation with a continuous slope is obtained. Numerically, its value is equal to the inhibition efficiency obtained using Eq. (15). In addition, as we can see from Fig. 4, at 25°C, we obtain a straight line with a correlation coefficient (R^2) greater than 0.98. This indicates the adsorption of this inhibitor in an H_2S-containing environment following the Langmuir adsorption isotherm. The Langmuir model is a standard model for various steel/inhibitor/electrolyte systems, in which the adsorbed mo-

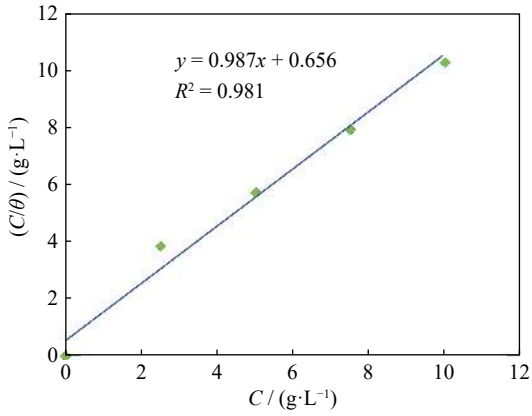

Fig. 4. Langmuir adsorption isotherm of the adsorption of different concentrations of 2-mercaptobenzothiazole on the surface of API X60 steel.

lecules occupy only one location on the metal surface [65–68].

Using the thermodynamic results obtained from the adsorption isotherms, we can determine the type of inhibitor adsorption (chemical or physical). In fact, using the K_{ads} values and Eq. (16), we can obtain the Gibbs free energy of the inhibitor ($\Delta G^{\ominus}_{ads}$) under different conditions, as follows [64]:

$$\Delta G^{\ominus}_{ads} = -RT\ln(1\times10^{6}K_{ads}) \quad (16)$$

where R is gas constant, and T is temperature. Table 3 shows the $\Delta G^{\ominus}_{ads}$ value, in which we can see that the $\Delta G^{\ominus}_{ads}$ value is negative. Negative $\Delta G^{\ominus}_{ads}$ value and high positive K_{ads} value indicate that the 2-mercaptobenzothiazole molecules are strongly and immediately adsorbed onto the surface of the API X60 pipeline steel [68–70]. Generally, a free energy of adsorption value of −20 kJ·mol^{-1} or lower is considered standard for the electrostatic adsorption process between inhibitor molecules and a steel surface (physical adsorption). A numerical value close to or higher than −40 kJ·mol^{-1} is considered to indicate sharing of the electrical charge and the transfer of electrons from organic molecules to the steel surface (chemical adsorption) [71–76].

Table 3. Calculated thermodynamic parameters for the adsorption of 2-mercaptobenzothiazole inhibitor on the surface of API X60 pipeline steel in an H_2S-containing environment

Temperature / °C	K_{ads} / (dm^3·mol^{-1})	$\Delta G^{\ominus}_{ads}$ / (kJ·mol^{-1})
25	1.524	−35.27482

Here, our assessment of $\Delta G^{\ominus}_{ads}$ shows that its value is lower than −20 kJ·mol^{-1} and higher than −40 kJ·mol^{-1}. Therefore, the adsorption of 2-mercaptobenzothiazole on the surface of the API X60 pipeline steel is in the form of physical–chemical adsorption. Also, as the $\Delta G^{\ominus}_{ads}$ has a negative value, we can conclude that the adsorption of 2-mercaptobenzothiazole on the surface of the pipeline steel occurs spontaneously.

3.4. Electrochemical impedance spectroscopy

EIS tests were performed to investigate the electrode/electrolyte interface and to evaluate the processes occurring on the surface with and without the 2-mercaptobenzothiazole inhibitor in the H_2S-containing environment. Fig. 5 shows Nyquist diagrams obtained from the EIS tests, in which we can observe that with increase in the concentration of the 2-mercaptobenzothiazole inhibitor, the diameter of the Nyquist plots increased significantly. This illustrates the excellent inhibitory performance of the 2-mercaptobenzothiazole inhibitor in preventing corrosion of the API X60 steel surface in H_2S-containing medium. Also, the shapes of the Nyquist plots are incomplete semicircles, with their centers below the real impedance axis. These incomplete semicircles formed by the Nyquist plots could be due to surface heterogeneity or corrosion control by the charge-transfer processes [77–79], which is known as the dispersive effect. The results obtained in this study reveal that at all concentrations of 2-mercaptobenzothiazole, the material has an inhibitory effect on the surface corrosion of API X60 pipeline steel.

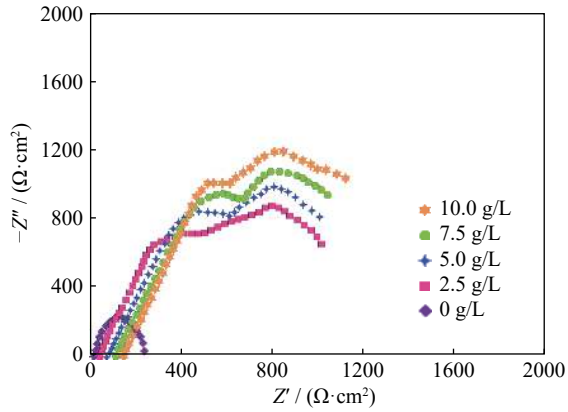

Fig. 5. Nyquist diagram showing the influence of the concentration of the 2-mercaptobenzothiazole inhibitor on the API X60 steel.

We used an electrical equivalent circuit to understand both the impedance and how the elements are positioned at the interface of the pipeline/electrolyte steel. The circuit in Fig. 6 shows two conditions: (a) without corrosion inhibitor and (b) with corrosion inhibitor. The elements of this equivalent circuit include the solution resistance (R_s), resistance of the film formed on the steel surface (R_f), constant phase element of the film formed on the steel surface (CPE_f), charge-transfer resistance of the electric double layer of steel (R_{ct}), and the constant phase element corresponding to the film formed on the electric double layer (CPE_{ct}). The electrochemical parameters are obtained by matching the impedance data with the equivalent circuit, as shown in Table 4. From Fig. 5 and Table 4, we can see that the decrease in the constant phase element (CPE) is proportional to the increase in the diameter of the Nyquist diagrams. As a result, it can be said that with the increase in the concentration of the inhibitor, the CPE decreased, which led to an increase in the diameter of the Nyquist plots. Eventually, this leads to higher corrosion resistance [80–83]. This decrease in the CPE can be attributed to a decrease in the local dielectric constant or an increase in the thickness of the electrical double layer. It also indicates the adsorption of 2-mercaptobenzothiazole inhibitor molecules at the pipeline steel/electrolyte interface as well as corrosion control by this inhibitor. Moreover, according to Table 4, it is evident that in the presence of 2-mercaptobenzothiazole inhibitor, the R_f values increase significantly relative to that without any inhibitor, and this increase is proportional to the

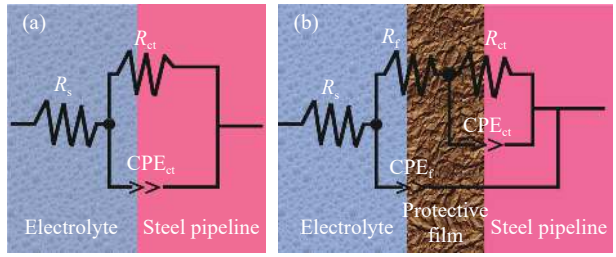

Fig. 6. Equivalent circuit matching of the Nyquist diagrams in the EIS tests (a) without corrosion inhibitor and (b) with corrosion inhibitors.

inhibitor concentration. In a sense, we can say that the adsorption of the inhibitor onto the surface of the API X60 pipeline steel is due to the formation of a very high-strength protective film. The resistance of this protective film increases with increase in the concentration of the 2-mercaptobenzothiazole inhibitor due to the increased adsorption of the inhibitor's molecules onto the surface. An assessment of the R_{ct} values reveals that by increasing the concentration of the 2-mercaptobenzothiazole inhibitor, the R_{ct} values increased due to the adsorption of the 2-mercaptobenzothiazole inhibitor on the surface of the API X60 pipeline steel, which changed the nature of the electrical double layer.

Table 4. Electrochemical parameters obtained by circuit matching of the Nyquist diagrams

Inhibitor concentration / ($g \cdot L^{-1}$)	R_s / ($\Omega \cdot cm^2$)	R_f / ($\Omega \cdot cm^2$)	Q_f / ($\mu\Omega \cdot s^n \cdot cm^{-2}$)	n_1	R_{ct} / ($\Omega \cdot cm^2$)	Q_{ct} / ($\mu\Omega \cdot s^n \cdot cm^{-2}$)	n_2
0	12 ± 4	—	—	0.57 ± 0.13	242 ± 8	294.267 ± 0.764	—
2.5	45 ± 7	406 ± 8	365.018 ± 0.371	0.79 ± 0.15	729 ± 9	188.657 ± 0.214	0.90 ± 0.08
5.0	69 ± 6	512 ± 7	302.382 ± 0.413	0.84 ± 0.12	746 ± 8	147.029 ± 0.620	0.92 ± 0.09
7.5	89 ± 8	561 ± 8	267.917 ± 0.246	0.89 ± 0.09	837 ± 9	89.613 ± 0.479	0.95 ± 0.11
10.0	107 ± 8	594 ± 9	206.842 ± 0.370	0.94 ± 0.17	948 ± 9	47.068 ± 0.708	0.98 ± 0.12

Note: Q_f is capacitor time constant for inhibitor film; n_1 is phase arctangent for inhibitor film; Q_{ct} is capacitor time constant for pipeline; n_2 is phase arctangent for pipeline.

Fig. 7(a) shows the Bode curves obtained from the EIS tests. The Bode Z curve ($|Z|$, based on frequency) of the pipeline steel with inhibitor protection is linear with the slope of −1. With the diffusion of destructive agents onto the surface of the pipeline steel, the slope of this curve changes. Subsequently, corrosion starts at the interface of the electrolyte and the surface of the pipeline steel. Generally, to determine the protective behavior of the film (the adsorption of the inhibitor onto the surface of the pipeline steel) and assess the parameters of this film, the slope of the Bode Z curve was studied [79–80]. Here, the Bode Z curves are substantially higher in the presence of different concentrations of 2-mercaptobenzothiazole, as compared to that in the absence of the 2-mercaptobenzothiazole inhibitor. This suggests that the surface of the API X60 steel is well protected by the 2-mercaptobenzothiazole inhibitor. However, a comparison of the Bode Z curves in Fig. 7(a) shows that the highest $|Z|$ occurs when using 10 g/L 2-mercaptobenzothiazole inhibitor. These results match well with those obtained from the OCP tests, potentiodynamic polarization tests, and the Nyquist plots. The Bode phase plots in Fig. 7(b) show that these curves range from the phase angles of −30° to −85° with 2-mercaptobenzothiazole inhibitor as compared to that without inhibitor. As such, we can conclude that the pipeline steel is protected by 2-mercaptobenzothiazole in the sour environment, and has high resistance and low capacity [79–80]. In fact, the adsorbed inhibitor on the surface of the pipeline steel acts as a barrier against the attack of the ions and prevents diffusion of the electrolyte into the surface of the steel. Considering the general electrochemical behavior indicated by the Bode phase curves, we know that the protection of the API X60 pipeline steel by the 2-mercaptobenzothiazole inhibitor in the sour environment is almost the same as that under different conditions, with the only difference being its lower or higher resistance. Generally, during the immersion of pipeline steel in an electrolyte, the protective film that forms is saturated with the solution, which forms an ionic conduction pathway in the film for the passage of destructive ions to the pipeline surface. Therefore, the greater is the adsorption of the inhibitor on the surface of the steel, the greater is the adhesion between the inhibitor and the surface, and the smaller is the pathway for the diffusion of the attacking ions and thus the lower is the corrosion rate. Given the EIS results, all concentrations of 2-mercaptobenzothiazole provided barrier-type protection. However, their efficiency increased with increase in the concentration of 2-mercaptobenzothiazole due to the reduction in the attacking ions. In the Bode phase plots of Fig. 7(b), there are two maximum

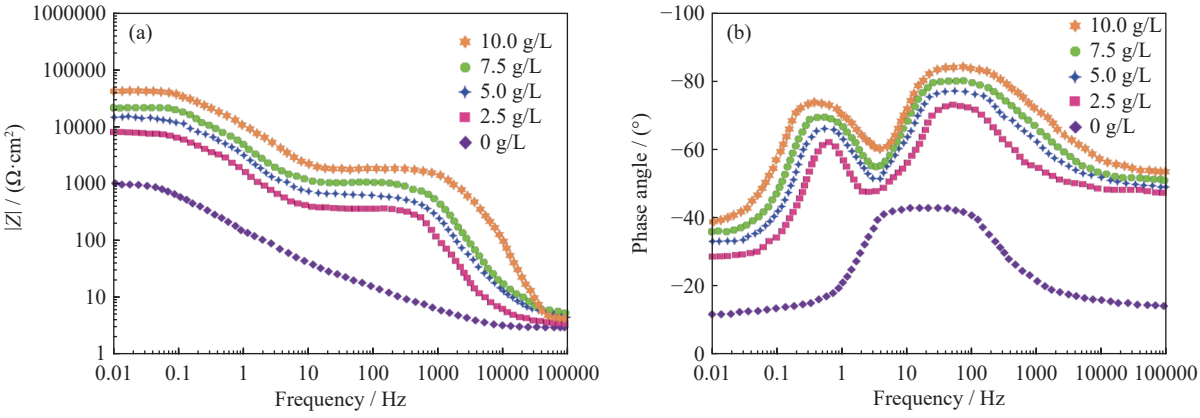

Fig. 7. EIS tests curves: (a) Bode *Z* curves; (b) Bode phase curves.

phase values with the 2-mercaptobenzothiazole inhibitor, but one maximum phase value without the 2-mercaptobenzothiazole inhibitor. This suggests the presence of two time constants for the condition with the 2-mercaptobenzothiazole inhibitor, but one for that without the 2-mercaptobenzothiazole inhibitor.

3.5. Examination of the corrosion products and morphology

We used SEM to evaluate the morphology and corrosion products formed on the surface of the API X60 pipeline in the H_2S-containing environment. We performed this test at the end of the potentiodynamic polarization test in an environment containing 10 g/L of 2-mercaptobenzothiazole inhibitor. EDS analysis of the corrosion products was also used to measure the local quantities of the constituents of the protective film. Using this procedure enables the assessment of the corrosion mechanism proposed by the electrochemical methods. Fig. 8 shows an SEM micrograph and EDS analysis of the API X60 pipeline steel surface tested in an H_2S-containing environment with 10 g/L of 2-mercaptobenzothiazole inhibitor. In the figure, it appears that the failure of the passive film occurs by the formation of a relatively large hole on the surface of the API X60 pipeline steel, along with a substantial amount of sediment around the cavity. In addition, as shown in Fig. 8, the formation of a non-stick protective film is evident on the surface of the API X60 pipeline steel, the composition of which includes elements such as sulfur, iron, and oxygen. The presence of different amounts of sulfur in the surface film points to the occurrence of H_2S corrosion on the surface of the API X60 pipeline steel. In fact, it is known that a sour-corrosion mechanism is activated on the surface of the API X60 pipeline steel due to the formation of an iron sulfide film. In general, the structure and shielding of an iron sulfide film is dependent on the concentration of hydrogen sulfide in the environment. Overall, the environmental factors, production conditions, and microstructural characteristics have a synergetic influence on the properties (e.g., mechanical and corrosion properties) of strategic engineering components [84–89].

Fig. 9 shows an SEM micrograph and EDS analysis of the surface of API X60 steel tested in an H_2S environment without the 2-mercaptobenzothiazole inhibitor. We can see that no surface film formed on the surface of the steel. In fact, as depicted in this figure, the surface of the steel is severely damaged, and this damage is uniformly distributed over the surface of the steel. A comparison of the amount of damage in Figs. 8 and 9 indicates that with the inhibitor, the steel surface experiences much less damage than without the inhibitor. These observations match well with the corrosion rates obtained from the electrochemical tests. We can also see in the EDS spectrum that the corrosion products on the surface

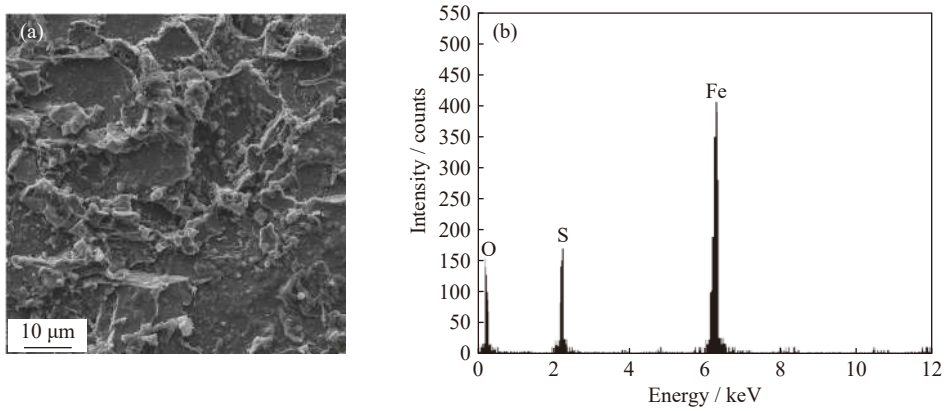

Fig. 8. (a) SEM micrograph and (b) EDS analysis of the API X60 steel surface tested in H_2S-containing environment containing 10 g/L 2-mercaptobenzothiazole inhibitor.

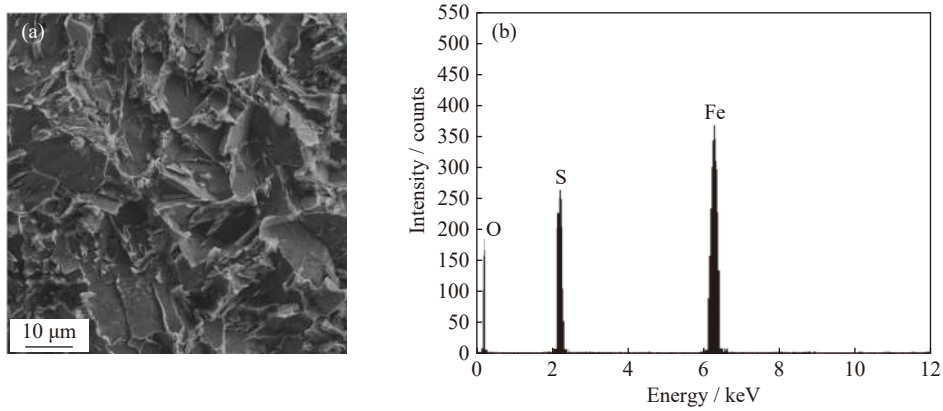

Fig. 9. (a) SEM micrograph and (b) EDS analysis of the surface of the API X60 steel tested in an H_2S environment without 2-mercaptobenzothiazole inhibitor.

of the steel contain the elements sulfur, iron, and oxygen. The presence of the various amount of the sulfur in the analysis of the corrosion products is indicative of the presence of H_2S on the surface of the API X60 pipeline steel.

4. Conclusions

In this study, we investigated the effect of the 2-mercaptobenzothiazole concentration on the sour-corrosion behavior of API X60 pipeline steel in an H_2S-containing environment. We evaluated the corrosion behavior of API X60 pipeline steel in H_2S-containing environment at 25°C in the presence of 0, 2.5, 5.0, 7.5, and 10.0 g/L of 2-mercaptobenzothiazole inhibitor. OCP, potentiodynamic polarization, and EIS tests were performed to determine the corrosion behavior of the API X60 pipeline steel in these conditions. SEM and EDS analyses were also performed to identify the corrosion products formed on the surface of this steel. The results of this study are as follows:

(1) Our examination of the OCP curves revealed that the OCP shifted to a much more negative value in the absence of the 2-mercaptobenzothiazole inhibitor. However, in the presence of the 2-mercaptobenzothiazole inhibitor, potential changes and fluctuations in the OCP curves showed an upward trend, which indicated the formation of a protective film on the API X60 pipeline surface.

(2) The corrosion potential displacement was determined to be greater than 85 mV with increase in the concentration of 2-mercaptobenzothiazole in an H_2S-containing environment. Therefore, we can conclude that 2-mercaptobenzothiazole in an H_2S-containing medium is an anodic or cathodic potential inhibitor for API X60 steel.

(3) Our evaluation of the potentiodynamic polarization curves showed that the inhibition efficiency and surface area increased with increase in the concentration of 2-mercaptobenzothiazole in the H_2S-containing environment. Under these circumstances, the corrosion current density and corrosion rate of the API X60 steel decreased.

(4) In the potentiodynamic polarization curves, the current densities in both the cathodic and anodic branches of the Tafel curves decreased in the presence of 2-mercaptobenzothiazole in the H_2S-containing environment, compared to those in the absence of 2-mercaptobenzothiazole in the H_2S-containing environment. This reflects the effect of 2-mercaptobenzothiazole on both the cathodic and anodic reactions of the API X60 pipeline steel, as well as its complex inhibitory mechanism.

(5) Based on verification of the Langmuir adsorption isotherm, we found that the 2-mercaptobenzothiazole inhibitor adsorbed onto the API X60 steel surface in the H_2S-containing environment followed a Langmuir adsorption isotherm.

(6) The $\Delta G^{\ominus}_{ads}$ analysis showed that the value was determined to be less than −20 kJ·mol^{-1} and more than −40 kJ·mol^{-1}. Therefore, the adsorption of 2-mercaptobenzothiazole on the surface of the API X60 pipeline steel was both physical and chemical. Also, as the $\Delta G^{\ominus}_{ads}$ showed a value was negative, we concluded that the adsorption 2-mercaptobenzothiazole on the surface of the pipeline steel was spontaneous.

(7) Examination of the Nyquist plots showed that 2-mercaptobenzothiazole at all concentrations had an inhibitory effect on the surface corrosion of the API X60 pipeline steel. According to these plots, increase in the concentration of 2-mercaptobenzothiazole inhibitor significantly increased the diameters of the Nyquist plots, which indicates the excellent inhibitory performance of the 2-ercaptobenzothiazole inhibitor in preventing corrosion of API X60 steel surfaces in an H_2S-containing environment.

(8) An analysis of the corrosion products showed that iron sulfide compounds had formed on the surface of the steel.

Conflict of Interest

All authors declared that they have no conflict of interest.

References

[1] Q. Sun, C.F. Chen, X. Zhao, H. Chi, Y. He, Y.C. Li, Y.M. Qi, and H.B. Yu, Ion-selectivity of iron sulfides and their effect on H_2S corrosion, *Corros. Sci.*, 158(2019), art. No. 108085.

[2] M.D.D. Ayagou, G.R. Joshi, T.T.M. Tran, B. Tribollet, E. Sutter, C. Mendibide, C. Duret-Thual, and J. Kittel, Impact of oxygen contamination on the electrochemical impedance spectroscopy of iron corrosion in H_2S solutions, *Corros. Sci.*, 164(2020), art. No. 108302.

[3] C. Mendibide and C. Duret-Thual, Determination of the critical pitting temperature of corrosion resistant alloys in H_2S containing environments, *Corros. Sci.*, 142(2018), p. 56.

[4] Z.G. Liu, X.H. Gao, L.X. Du, J.P. Li, P. Li, C. Yu, R.D.K. Misra, and Y.X. Wang, Comparison of corrosion behaviour of low-alloy pipeline steel exposed to H_2S/CO_2-saturated brine and vapour-saturated H_2S/CO_2 environments, *Electrochim. Acta*, 232(2017), p. 528.

[5] R.S. Feng, J. Beck, M. Ziomek-Moroz, and S.N. Lvov, High-temperature electrochemical corrosion of ultra-high strength carbon steel in H_2S-containing alkaline brines, *Electrochim. Acta*, 241(2017), p. 341.

[6] H. Xu, S.K. Zhou, Y.M. Zhu, W.G. Xu, X.H. Xiong, and H.Z. Tan, Experimental study on the effect of H_2S and SO_2 on high temperature corrosion of 12Cr1MoV, *Chin. J. Chem. Eng.*, 27(2019), No. 8, p. 1956.

[7] I.B. Obot, M.M. Solomon, S.A. Umoren, R. Suleiman, M. Elanany, N.M. Alanazi, and A.A. Sorour, Progress in the development of sour corrosion inhibitors: Past, present, and future perspectives, *J. Ind. Eng. Chem.*, 79(2019), p. 1.

[8] A.F. Avelino, W.S. Araújo, D.F. Dias, L.P.M. dos Santos, A.N. Correia, and P. de Lima-Neto, Corrosion investigation of the 18Ni 300 grade maraging steel in aqueous chloride medium containing H_2S and CO_2, *Electrochim. Acta*, 286(2018), p. 339.

[9] J. Ning, Y.G. Zheng, D. Young, B. Brown, and S. Nešić, Thermodynamic study of hydrogen sulfide corrosion of mild steel, *Corrosion*, 70(2014), No. 4, p. 375.

[10] S.J. Gao, B. Brown, D. Young, and M. Singer, Formation of iron oxide and iron sulfide at high temperature and their effects on corrosion, *Corros. Sci.*, 135(2018), p. 167.

[11] C. Rémazeilles, D. Neff, J.A. Bourdoiseau, R. Sabot, M. Jeannin, and P. Refait, Role of previously formed corrosion product layers on sulfide-assisted corrosion of iron archaeological artefacts in soil, *Corros. Sci.*, 129(2017), p. 169.

[12] S. Grousset, M. Bayle, A. Dauzeres, D. Crusset, V. Deydier, Y. Linard, P. Dillmann, F. Mercier-Bion, and D. Neff, Study of iron sulphides in long-term iron corrosion processes: Characterisations of archaeological artefacts, *Corros. Sci.*, 112(2016), p. 264.
[13] G.M. Jiang, E. Wightman, B.C. Donose, Z.G. Yuan, P.L. Bond, and J. Keller, The role of iron in sulfide induced corrosion of sewer concrete, *Water Res.*, 49(2014), p. 166.
[14] X. Cai, X.E. Zhao, and H.Q. Yao, Spontaneous combustion tendency of iron sulfide corrosion: Oxidation characterization and thermostability, *Procedia Eng.*, 84(2014), p. 356.
[15] S.Q. Chen, Y.F. Cheng, and G. Voordouw, A comparative study of corrosion of 316L stainless steel in biotic and abiotic sulfide environments, *Int. Biodeterior. Biodegrad.*, 120(2017), p. 91.
[16] M. Asadian, M. Sabzi, and S.H.M. Anijdan, The effect of temperature, CO_2, H_2S gases and the resultant iron carbonate and iron sulfide compounds on the sour corrosion behaviour of ASTM A-106 steel for pipeline transportation, *Int. J. Press. Vessels Pip.*, 171(2019), p. 184.
[17] P.P. Bai, J. Zhou, B.W. Luo, S.Q. Zheng, P.Y. Wang, and Y. Tian, Hydrogen embrittlement of X80 pipeline steel in H_2S environment: Effect of hydrogen charging time, hydrogen-trapped state and hydrogen charging–releasing–recharging cycles, *Int. J. Miner. Metall. Mater.*, 27(2020), No. 1, p. 63.
[18] K.X. Liao, F.L. Zhou, X.Q. Song, Y.R. Wang, S. Zhao, J.J. Liang, L. Chen, and G.X. He, Synergistic effect of O_2 and H_2S on the corrosion behavior of N80 steel in a simulated high-pressure flue gas injection system, *J. Mater. Eng. Perform.*, 29(2020), No. 1, p. 155.
[19] S.H.M. Anijdan, M. Sabzi, M. Asadian, and H.R. Jafarian, Effect of sub-layer temperature during HFCVD process on morphology and corrosion behavior of tungsten carbide coating, *Int. J. Appl. Ceram. Technol.*, 16(2019), No. 1, p. 243.
[20] T.R. Tamilarasan, R. Rajendran, G. Rajagopal, and J. Sudagar, Effect of surfactants on the coating properties and corrosion behaviour of Ni–P–nano-TiO_2 coatings, *Surf. Coat. Technol.*, 276(2015), p. 320.
[21] S.H.M. Anijdan, M. Sabzi, M.R. Zadeh, and M. Farzam, The effect of electroless bath parameters and heat treatment on the properties of Ni–P and Ni–P–Cu composite coatings, *Mater. Res.*, 21(2018), No. 2, art. No. e20170973.
[22] S.M. Dezfuli and M. Sabzi, Deposition of ceramic nanocomposite coatings by electroplating process: A review of layer-deposition mechanisms and effective parameters on the formation of the coating, *Ceram. Int.*, 45(2019), No. 17, p. 21835.
[23] A. Shahriari and H. Aghajani, Electrophoretic deposition of 3YSZ coating on AZ91D using an aluminum interlayer, *Prot. Met. Phys. Chem. Surf.*, 53(2017), No. 3, p. 518.
[24] M. Sabzi and S.H.M. Anijdan, Microstructural analysis and optical properties evaluation of sol–gel heterostructured NiO–TiO_2 film used for solar panels, *Ceram. Int.*, 45(2019), No. 3, p. 3250.
[25] M. Sabzi, S.H.M. Anijdan, and M. Asadian, The effect of substrate temperature on microstructural evolution and hardenability of tungsten carbide coating in hot filament chemical vapor deposition, *Int. J. Appl. Ceram. Technol.*, 15(2018), No. 6, p. 1350.
[26] A. Shahriari and H. Aghajani, Electrophoretic deposition of 3YSZ coating on AZ91D alloy using Al and Ni–P interlayers, *J. Mater. Eng. Perform.*, 25(2016), No. 10, p. 4369.
[27] M. Sabzi, S.H.M. Anijdan, M.R. Zadeh, and M. Farzam, The effect of heat treatment on corrosion behaviour of Ni–P–3 gr/lit Cu nano-composite coating, *Can. Metall. Q.*, 57(2018), No. 3, p. 350.
[28] S.M. Dezfuli and M. Sabzi, Deposition of self-healing thin films by the sol–gel method: A review of layer-deposition mechanisms and activation of self-healing mechanisms, *Appl. Phys. A*, 125(2019), No. 8, art. No. 557.
[29] T.R. Tamilarasan, U. Sanjith, R. Rajendran, G. Rajagopal, and J. Sudagar, Effect of reduced graphene oxide reinforcement on the wear characteristics of electroless Ni–P coatings, *J. Mater. Eng. Perform.*, 27(2018), No. 6, p. 3044.
[30] M. Sabzi, A. Obeydavi, and S.H.M. Anijdan, The effect of joint shape geometry on the microstructural evolution, fracture toughness, and corrosion behavior of the welded joints of a Hadfield steel, *Mech. Adv. Mater. Struct.*, 26(2019), No. 12, p. 1053.
[31] E. Ohaeri, J. Omale, U. Eduok, J. Szpunar, M. Arafin, and F. Fazeli, Effect of microstructure and texture evolution on the electrochemical corrosion behavior of warm-rolled API 5L X70 pipeline steel, *Metall. Mater. Trans. A*, 51(2020), No. 5, p. 2255.
[32] S.H.M. Anijdan and M. Sabzi, The evolution of microstructure of an high Ni HSLA X100 forged steel slab by thermomechanical controlled processing, [in] *The TMS 2018 Annual Meeting & Exhibition*, Phoenix, 2018, p. 145.
[33] D. Snihirova, S.V. Lamaka, P. Taheri, J.M.C. Mol, and M.F. Montemor, Comparison of the synergistic effects of inhibitor mixtures tailored for enhanced corrosion protection of bare and coated AA2024-T3, *Surf. Coat. Technol.*, 303(2016), p. 342.
[34] Z.X. Li, Q.L. Yu, C.Y. Zhang, Y.P. Liu, J. Liang, D.A. Wang, and F. Zhou, Synergistic effect of hydrophobic film and porous MAO membrane containing alkynol inhibitor for enhanced corrosion resistance of magnesium alloy, *Surf. Coat. Technol.*, 357(2019), p. 515.
[35] S.A.M. Refaey, F. Taha, and A.M.A. El-Malak, Inhibition of stainless steel pitting corrosion in acidic medium by 2-mercaptobenzoxazole, *Appl. Surf. Sci.*, 236(2004), No. 1-4, p. 175.
[36] N. Gladkikh, Y. Makarychev, M. Maleeva, M. Petrunin, L. Maksaeva, A. Rybkina, A. Marshakov, and Y. Kuznetsov, Synthesis of thin organic layers containing silane coupling agents and azole on the surface of mild steel. Synergism of inhibitors for corrosion protection of underground pipelines, *Prog. Org. Coat.*, 132(2019), p. 481.
[37] N. Kovačević and A. Kokalj, Chemistry of the interaction between azole type corrosion inhibitor molecules and metal surfaces, *Mater. Chem. Phys.*, 137(2012), No. 1, p. 331.
[38] P.C. Okonkwo, E. Ahmed, and A.M.A. Mohamed, Effect of temperature on the corrosion behavior of API X80 steel pipeline, *Int. J. Electrochem. Sci.*, 10(2015), No. 12, p. 10246.
[39] H.Y. Cen, J.J. Cao, Z.Y. Chen, and X.P. Guo, 2-Mercaptobenzothiazole as a corrosion inhibitor for carbon steel in supercritical CO_2–H_2O condition, *Appl. Surf. Sci.*, 476(2019), p. 422.
[40] I.A. Kartsonakis, A.C. Balaskas, E.P. Koumoulos, C.A. Charitidis, and G.C. Kordas, Incorporation of ceramic nanocontainers into epoxy coatings for the corrosion protection of hot dip galvanized steel, *Corros. Sci.*, 57(2012), p. 30.
[41] M.A. Lucio-Garcia, J.G. Gonzalez-Rodriguez, M. Casales, L. Martinez, J.G. Chacon-Nava, M.A. Neri-Flores, and A. Martinez-Villafañe, Effect of heat treatment on H_2S corrosion of a micro-alloyed C–Mn steel, *Corros. Sci.*, 51(2009), No. 10, p. 2380.
[42] S.M. Dezfuli and M. Sabzi, Effect of yttria and benzotriazole doping on wear/corrosion responses of alumina-based nanostructured films, *Ceram. Int.*, 44(2018), No. 16, p. 20245.
[43] M. Sabzi, S.M. Far, and S.M. Dezfuli, Effect of melting temperature on microstructural evolutions, behavior and corrosion morphology of Hadfield austenitic manganese steel in the casting process, *Int. J. Miner. Metall. Mater.*, 25(2018), No. 12, p. 1431.
[44] M. Sabzi, S.M. Dezfuli, and S.M. Far, Deposition of Ni–tungsten carbide nanocomposite coating by TIG welding: Characterization and control of microstructure and wear/corrosion re-

sponses, *Ceram. Int.*, 44(2018), No. 18, p. 22816.
[45] M. Sabzi and S.M. Dezfuli, A study on the effect of compositing silver oxide nanoparticles by carbon on the electrochemical behavior and electronic properties of zinc–silver oxide batteries, *Int. J. Appl. Ceram. Technol.*, 15(2018), No. 6, p. 1446.
[46] M. Sabzi, S.M. Dezfuli, M. Asadian, A. Tafi, and A. Mahaab, Study of the effect of temperature on corrosion behavior of galvanized steel in seawater environment by using potentiodynamic polarization and EIS methods, *Mater. Res. Express*, 6(2019), No. 7, art. No. 076508.
[47] H. Huang and W.J.D. Shaw, Electrochemical aspects of cold work effect on corrosion of mild steel in sour gas environments, *Corrosion*, 48(1992), No. 11, p. 931.
[48] R.J. Xiao, G.Q. Xiao, B. Huang, J.H. Feng, and Q.H. Wang, Corrosion failure cause analysis and evaluation of corrosion inhibitors of Ma Huining oil pipeline, *Eng. Fail. Anal.*, 68(2016), p. 113.
[49] A. Fragiel, S. Serna, J. Malo-Tamayo, P. Silva, B. Campillo, E. Martínez-Martínez, L. Cota, M.H. Staia, E.S. Puchi-Cabrera, and R. Perez, Effect of microstructure and temperature on the stress corrosion cracking of two microalloyed pipeline steels in H_2S environment for gas transport, *Eng. Fail. Anal.*, 105(2019), p. 1055.
[50] T. Yan, S.T. Zhang, L. Feng, Y.J. Qiang, L.S. Lu, D.L. Fu, Y.N. Wen, J.D. Chen, W.P. Li, and B.C. Tan, Investigation of imidazole derivatives as corrosion inhibitors of copper in sulfuric acid: Combination of experimental and theoretical researches, *J. Taiwan Inst. Chem. Eng.*, 106(2020), p. 118.
[51] H. Yang, W.H. Li, X.Y. Liu, A. Liu, P. Hang, R. Ding, T. Li, Y.M. Zhang, W. Wang, and C.S. Xiong, Preparation of corrosion inhibitor loaded zeolites and corrosion resistance of carbon steel in simulated concrete pore solution, *Constr. Build. Mater.*, 225(2019), p. 90.
[52] D.S. Chauhan, A.M. Kumar, and M.A. Quraishi, Hexamethylenediamine functionalized glucose as a new and environmentally benign corrosion inhibitor for copper, *Chem. Eng. Res. Des.*, 150(2019), p. 99.
[53] D.D. Wang, Q. Zhu, Y.Y. Su, J. Li, A.W. Wang, and Z.P. Xing, Preparation of MgAlFe-LDHs as a deicer corrosion inhibitor to reduce corrosion of chloride ions in deicing salts, *Ecotoxicol. Environ. Saf.*, 174(2019), p. 164.
[54] C. Verma, H. Lgaz, D.K. Verma, E.E. Ebenso, I. Bahadur, and M.A. Quraishi, Molecular dynamics and Monte Carlo simulations as powerful tools for study of interfacial adsorption behavior of corrosion inhibitors in aqueous phase: A review, *J. Mol. Liq.*, 260(2018), p. 99.
[55] P. Arellanes-Lozada, O. Olivares-Xometl, N.V. Likhanova, I.V. Lijanova, J.R. Vargas-García, and R.E. Hernández-Ramírez, Adsorption and performance of ammonium-based ionic liquids as corrosion inhibitors of steel, *J. Mol. Liq.*, 265(2018), p. 151.
[56] S.K. Shukla, M.A. Quraishi, and E. Ebenso, Adsorption and corrosion inhibition properties of cefadroxil on mild steel in hydrochloric acid, *Int. J. Electrochem. Sci.*, 6(2011), No. 7, p. 2912.
[57] S.T. Zhang, Z.H. Tao, S.G. Liao, and F.J. Wu, Substitutional adsorption isotherms and corrosion inhibitive properties of some oxadiazol-triazole derivative in acidic solution, *Corros. Sci.*, 52(2010), No. 9, p. 3126.
[58] M. El Faydy, B. Lakhrissi, C. Jama, A. Zarrouk, L.O. Olasunkanmi, E.E. Ebenso, and F. Bentiss, Electrochemical, surface and computational studies on the inhibition performance of some newly synthesized 8-hydroxyquinoline derivatives containing benzimidazole moiety against the corrosion of carbon steel in phosphoric acid environment, *J. Mater. Res. Technol.*, 9(2020), No. 1, p. 727.
[59] M.E. Belghiti, S. Bouazama, S. Echihi, A. Mahsoune, A. Elmelouky, A. Dafali, K.M. Emran, B. Hammouti, and M. Tabyaoui, Understanding the adsorption of newly benzylideneaniline derivatives as a corrosion inhibitor for carbon steel in hydrochloric acid solution: Experimental, DFT and molecular dynamic simulation studies, *Arabian J. Chem.*, 13(2020), No. 1, p. 1499.
[60] M. Husaini, B. Usman, and M.B. Ibrahim, Study of corrosion inhibition of aluminum in nitric acid solution using anisaldehyde (4-methoxy benzaldehyde) as inhibitor, *Algerian J. Eng. Tech.*, 1(2019), No. 1, p. 11.
[61] C.X. Liang, Z. Liu, Q.Q. Liang, G.C. Han, J.X. Han, S.F. Zhang, and X.Z. Feng, Synthesis of 2-aminofluorene bis-Schiff base and corrosion inhibition performance for carbon steel in HCl, *J. Mol. Liq.*, 277(2019), p. 330.
[62] N.A. Negm, N.G. Kandile, E.A. Badr, and M.A. Mohammed, Gravimetric and electrochemical evaluation of environmentally friendly nonionic corrosion inhibitors for carbon steel in 1 M HCl, *Corros. Sci.*, 65(2012), p. 94.
[63] S.S. Shivakumar and K.N. Mohana, Corrosion behavior and adsorption thermodynamics of some Schiff bases on mild steel corrosion in industrial water medium, *Int. J. Corros.*, 2013(2013), art. No. 543204.
[64] S.A. Umoren, I.B. Obot, A. Madhankumar, and Z.M. Gasem, Performance evaluation of pectin as ecofriendly corrosion inhibitor for X60 pipeline steel in acid medium: Experimental and theoretical approaches, *Carbohydr. Polym.*, 124(2015), p. 280.
[65] M. Benabdellah, A. Tounsi, K.F. Khaled, and B. Hammouti, Thermodynamic, chemical and electrochemical investigations of 2-mercapto benzimidazole as corrosion inhibitor for mild steel in hydrochloric acid solutions, *Arabian J. Chem.*, 4(2011), No. 1, p. 17.
[66] H. El Moll, K.M. Alenezi, M.K. Abdel-Latif, H. Halouani, and M.M. EL-Deeb, Water-soluble Calix [4] arenes as inhibitors for the corrosion of aluminium in 2 M H_2SO_4 solution, *Int. J. Electrochem. Sci.*, 15(2020), p. 252.
[67] H. Hamani, T. Douadi, D. Daoud, M. Al-Noaimi, R.A. Rikkouh, and S. Chafaa, 1-(4-nitrophenylo-imino)-1-(phenylhydrazono)-propan-2-one as corrosion inhibitor for mild steel in 1 M HCl solution: Weight loss, electrochemical, thermodynamic and quantum chemical studies, *J. Electroanal. Chem.*, 801(2017), p. 425.
[68] D.K. Yadav, M.A. Quraishi, and B. Maiti, Inhibition effect of some benzylidenes on mild steel in 1 M HCl: An experimental and theoretical correlation, *Corros. Sci.*, 55(2012), p. 254.
[69] G. Avci, Corrosion inhibition of indole-3-acetic acid on mild steel in 0.5 M HCl, *Colloids Surf. A*, 317(2008), No. 1-3, p. 730.
[70] N.O. Obi-Egbedi and I.B. Obot, Inhibitive properties, thermodynamic and quantum chemical studies of alloxazine on mild steel corrosion in H_2SO_4, *Corros. Sci.*, 53(2011), No. 1, p. 263.
[71] A. Fawzy, M. Abdallah, I.A. Zaafarany, S.A. Ahmed, and I.I. Althagafi, Thermodynamic, kinetic and mechanistic approach to the corrosion inhibition of carbon steel by new synthesized amino acids-based surfactants as green inhibitors in neutral and alkaline aqueous media, *J. Mol. Liq.*, 265(2018), p. 276.
[72] H. Ouici, M. Tourabi, O. Benali, C. Selles, C. Jama, A. Zarrouk, and F. Bentiss, Adsorption and corrosion inhibition properties of 5-amino 1, 3, 4-thiadiazole-2-thiol on the mild steel in hydrochloric acid medium: Thermodynamic, surface and electrochemical studies, *J. Electroanal. Chem.*, 803(2017), p. 125.
[73] K. Adardour, R. Touir, M. El bakri, H. Larhzil, M.E. Touhami, Y. Ramli, A. Zarrouk, H. El Kafsaoui, and E.M. Essassi, Thermodynamic properties and comparative studies of quinoxaline derivatives as a corrosion inhibitor for mild steel in 1 M H_2SO_4, *Res. Chem. Intermed.*, 41(2015), No. 3, p. 1571.
[74] A.A.F. Sabirneeza and S. Subhashini, Poly(vinyl alcohol–proline) as corrosion inhibitor for mild steel in 1M hydrochloric acid, *Int. J. Ind. Chem.*, 5(2014), No. 3-4, p. 111.

[75] M.L. Gao, J. Zhang, Q.N. Liu, J.L. Li, R.J. Zhang, and G. Chen, Effect of the alkyl chain of quaternary ammonium cationic surfactants on corrosion inhibition in hydrochloric acid solution, *Comptes Rendus Chimie*, 22(2019), No. 5, p. 355.

[76] D.S. Zinad, M. Hanoon, R.D. Salim, S.I. Ibrahim, A.A. Al-Amiery, M.S. Takriff, and A.A.H. Kadhum, A new synthesized coumarin-derived Schiff base as a corrosion inhibitor of mild steel surface in HCl medium: Gravimetric and DFT studies, *Int. J. Corros. Scale Inhib.*, 9(2020), No. 1, p. 228.

[77] S.M. Dezfuli and M. Sabzi, A study on the effect of presence of CeO_2 and benzotriazole on activation of self-healing mechanism in ZrO_2 ceramic-based coating, *Int. J. Appl. Ceram. Technol.*, 15(2018.), No. 5, p. 1248.

[78] M. Sabzi and S.M. Dezfuli, Deposition of Al_2O_3 ceramic film on copper-based heterostructured coatings by aluminizing process: Study of the electrochemical responses and corrosion mechanism of the coating, *Int. J. Appl. Ceram. Technol.*, 16(2019), No. 1, p. 195.

[79] M. Sabzi, S.M. Dezfuli, and S.M. Mirsaeedghazi, The effect of pulse-reverse electroplating bath temperature on the wear/corrosion response of Ni–Co/tungsten carbide nanocomposite coating during layer deposition, *Ceram. Int.*, 44(2018), No. 16, p. 19492.

[80] M. Sabzi, S.M. Far, and S.M. Dezfuli, Characterization of bioactivity behavior and corrosion responses of hydroxyapatite-ZnO nanostructured coating deposited on NiTi shape memory alloy, *Ceram. Int.*, 44(2018), No. 17, p. 21395.

[81] S.H.M. Anijdan, M. Sabzi, M.R. Zadeh, and M. Farzam, The influence of pH, rotating speed and Cu content reinforcement nano-particles on wear/corrosion response of Ni–P–Cu nanocomposite coatings, *Tribol. Int.*, 127(2018), p. 108.

[82] M. Sabzi, S.H.M. Anijdan, M. Ghobeiti-Hasab, and M. Fatemi-Mehr, Sintering variables optimization, microstructural evolution and physical properties enhancement of nano-WC ceramics, *J. Alloys Compd.*, 766(2018), p. 672.

[83] S.H.M. Anijdan, M. Sabzi, M. Ghobeiti-Hasab, and A. Roshan-Ghiyas, Optimization of spot welding process parameters in dissimilar joint of dual phase steel DP600 and AISI 304 stainless steel to achieve the highest level of shear-tensile strength, *Mater. Sci. Eng. A*, 726(2018), p. 120.

[84] S.H.M Anijdan and M. Sabzi, The effect of pouring temperature and surface angle of vortex casting on microstructural changes and mechanical properties of 7050Al-3 wt% SiC composite, *Mater. Sci. Eng. A*, 737(2018), p. 230.

[85] M. Sabzi and S.M. Dezfuli, Post weld heat treatment of hypereutectoid Hadfield steel: Characterization and control of microstructure, phase equilibrium, mechanical properties and fracture mode of welding joint, *J. Manuf. Processes*, 34(2018), p. 313.

[86] M. Sabzi and M. Farzam, Hadfield manganese austenitic steel: A review of manufacturing processes and properties, *Mater. Res. Express*, 6(2019), No. 10, art. No. 1065c2.

[87] M. Sabzi and S.M. Dezfuli, Drastic improvement in mechanical properties and weldability of 316L stainless steel weld joints by using electromagnetic vibration during GTAW process, *J. Manuf. Processes*, 33(2018), p. 74.

[88] M. Sabzi, S.M. Dezfuli, and Z. Balak, Crystalline texture evolution, control of the tribocorrosion behavior, and significant enhancement of the abrasion properties of a Ni–P nanocomposite coating enhanced by zirconia nanoparticles, *Int. J. Miner. Metall. Mater.*, 26(2019), No. 8, p. 1020.

[89] S.H.M. Anijdan and M. Sabzi, The effect of heat treatment process parameters on mechanical properties, precipitation, fatigue life, and fracture mode of an austenitic Mn Hadfield steel, *J. Mater. Eng. Perform.*, 27(2018), No. 10, p. 5246.